Corrections

Arthur T. Motta,[1] *Donald R. Olander,*[1] *and Albert J. Machiels*[2]

Electron Irradiation-Induced Amorphization of Precipitates in Zircaloy-2

REFERENCE: Motta, A. T., Olander, D. R., and Machiels, A. J., **"Electron Irradiation-Induced Amorphization of Precipitates in Zircaloy-2,"** *Effects of Radiation on Materials: 14th International Symposium, Volume I, ASTM STP 1046,* N. H. Packan, R. E. Stoller, and A. S. Kumar, Eds., American Society for Testing and Materials, Philadelphia, 1989, pp. 457–469.

ABSTRACT: The crystalline-amorphous transformation of $Zr_2(Ni,Fe)$ precipitates in Zircaloy by electron irradiation has been studied in the high voltage electron microscope at temperatures ranging from 92 to 283 K and dose rates between 10^{-3} and 4×10^{-2} dpa/s. The dose-to-amorphization was found to increase exponentially with temperature and to decrease with increasing dose rate. The occurrence of the transformation was modeled by calculating the increase in free energy because of irradiation effects: accumulation of point defects and lattice disordering. The time-dependent diffusion equation with recombination was solved to find the interstitial and vacancy concentrations as functions of dose, dose rate, and temperature. Random recombination was the assumed disordering mechanism. The transformation was assumed to occur when the free energy increase of the crystalline phase became equal to the difference in free energy between the amorphous state and the unirradiated crystal. The dose-to-amorphization predicted by the model agreed well with experimental results for reasonable values of the fitting parameters.

KEY WORDS: Zircaloy-2, crystalline-amorphous transformation, irradiation effects, energy

Zircaloy is widely used in the nuclear industry as a fuel cladding material because of its good mechanical, thermal, and nuclear properties. Its microstructure includes the intermetallic precipitates $Zr_2(Ni,Fe)$ and $Zr(Cr,Fe)_2$. Changes in the density, size, and composition of the precipitates alter the matrix concentrations of the minor alloying elements. In addition, the precipitates undergo a crystalline to amorphous (C-A) transformation under irradiation. These morphological changes may affect the mechanical and corrosion properties of the alloy.

Neutron irradiation-induced changes in these precipitates have been reported, including dissolution and amorphization [*1,2*]. The amorphization occurs at doses between 1 and 10 dpa at reactor operating temperatures and dose rates. The present study was conducted to investigate the effects of temperature and dose rate on the C-A transformation using electron irradiation. An attempt was also made to determine whether the C-A transformation occurs suddenly at a critical dose or whether the process is gradual. The results obtained are explained in terms of a model that relates the dose to amorphization with the temperature and the dose rate.

[1] University of California at Berkeley, Berkeley, CA.
[2] Electric Power Research Institute, Palo Alto, CA.

Experimental Procedure

Thin foils for transmission electron microscopy (TEM) were prepared from Zircaloy-2 rods furnished by Teledyne Wah-Chang of Albany, OR. Disks 3 mm in diameter and approximately 0.05-mm thick were obtained by mechanical polishing and punching. The specimens were then polished using a standard Fischione unit with a solution of 10% perchloric acid ($HClO_4$) in methanol at 25 V and 223 K.

The irradiations were performed at temperatures ranging from 92 to 283 K in the Kratos 1.5 MeV high voltage electron microscope (HVEM) at the National Center for Electron Microscopy (NCEM) at Lawrence Berkeley Laboratory. The vacuum was better than 10^{-7} torr. The electron flux density was calculated by measuring the beam current and the beam spot size. Diffraction patterns were taken at regular intervals to ascertain the occurrence of the transformation. The irradiated specimens were further examined for composition variations (solute segregation, precipitate dissolution) in a Philips EM400 with an EDX attachment.

To investigate the kinetics of the transformation, a series of diffraction patterns taken during irradiation was digitized and the images thus obtained further processed using the SEMPER software package at the NCEM. The fluence in dpa was calculated according to

$$\text{dpa}(t) = \sigma_d \Phi t \tag{1}$$

where t is the irradiation time (s), Φ is the flux density (e/cm^2s) and σ_d is the displacement cross section for electrons given by Oen [*3*], assuming a displacement energy of 40 eV as recommended in the ASTM Standard Recommended Practice for Neutron Radiation Simulation by Charged-Particle Irradiation (E 521-83).

The dose rate $k(\text{dpa/s}) = \sigma_d \Phi$ was corrected for the radial dependence of beam shape by multiplying the measured current density by the ratio R

$$R = \frac{\text{current density in central 0.3 } \mu \text{ spot}}{\text{current density in whole spot}} \tag{2}$$

Beam heating was taken into account by performing a heat transfer calculation for a simplified foil geometry. The temperature corrections thus obtained were of the order of 10 K, which agrees well with the literature [*4*].

Results

Figure 1 shows a cluster of $Zr_2(Ni,Fe)$ and $Zr(Cr,Fe)_2$ precipitates before and after amorphization as evidenced by the inset diffraction patterns. The experimental results for $Zr_2(Fe,Ni)$ are summarized in Fig. 2. The dose to amorphization is plotted against temperature for several values of the dose rate. The dose to amorphization at 92 K (not shown in Fig. 2) was found to be comparable to the result previously obtained by Morita et al. [*4*] with bulk zirconium nitrite (Zr_2Ni). The general form of the curve agrees qualitatively with results from the literature [*5,6*] in that the dose to amorphization rises exponentially at a definite temperature. There is also a tendency for the dose to amorphization is smaller for higher dose rates.

The precipitate dissolution and iron depletion that are present in neutron irradiation [*1,2*] were not observed in this study.

The occurrence of the amorphous transformation was followed by observing the transition

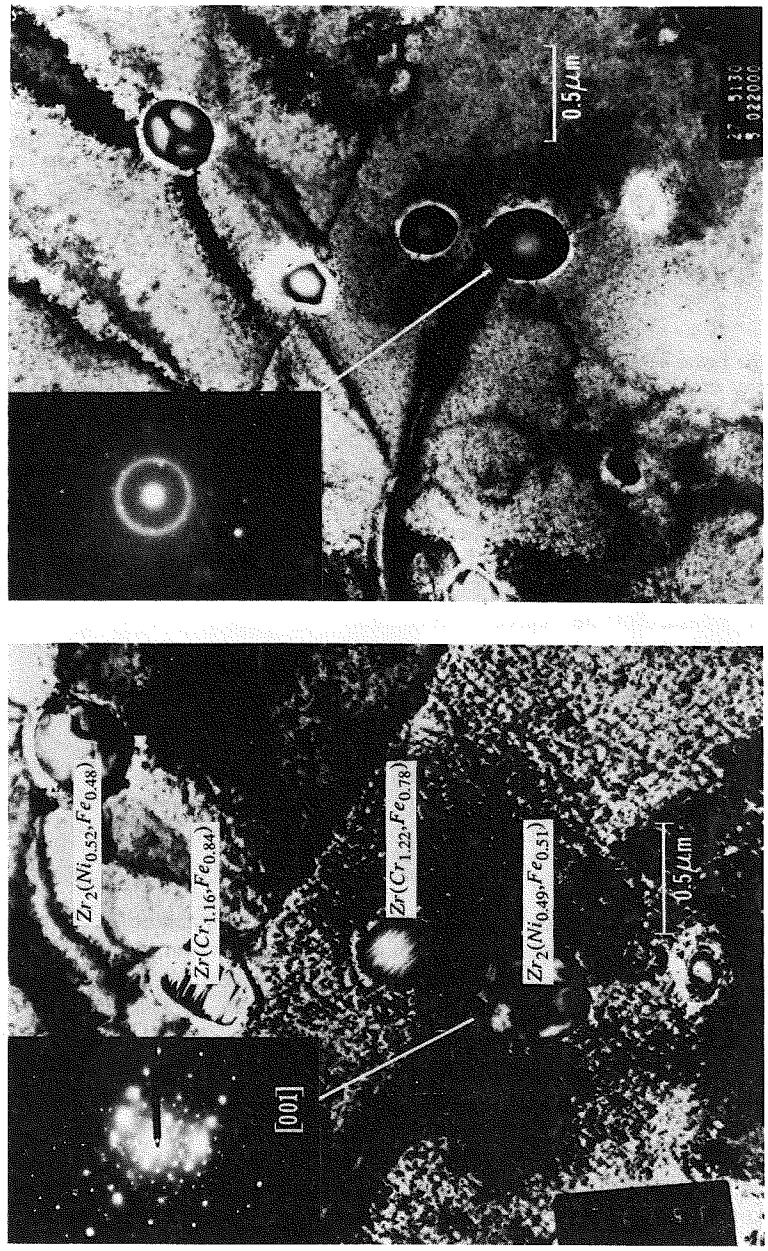

FIG. 1—*Amorphization of precipitates in Zircaloy-2. Precipitates are crystalline in* (a), *before irradiation. In* (b) *both* a *and* b *precipitates are amorphous, while* c *is partially amorphous (lower half) and* d *is still crystalline. The composition of the precipitates does not change from Fig. 1a to* b.

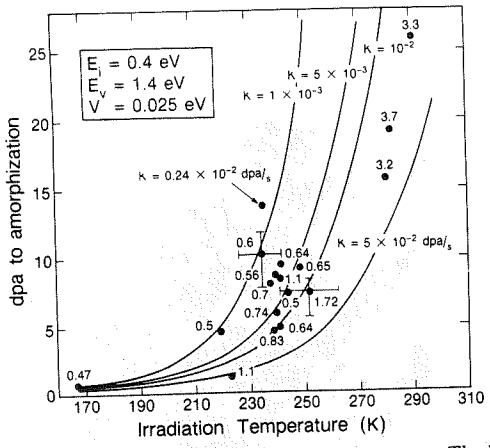

FIG. 2—*The figure shows dpa to amorphization versus temperature. The* k *values (in dpa/s* $\times$ 10^2*) are indicated for each data point. The solid curves are the fits obtained from Eq 5 and 37.*

from a spot pattern to a ring pattern. A sequence of diffraction patterns and their intensity maps is shown in Fig. 3. At first there is only the spot pattern (a), but as the fluence rises, the intensity of the spot pattern diminishes, and a ring pattern characteristic of the amorphous phase appears and grows stronger (b),(c), until only the ring pattern is left (d).

From the intensity maps shown in Fig. 3, one can obtain the parameter ψ, which is an experimental measure of the degree of crystallinity as a function of fluence. For a given beam current, the diffracted intensity and therefore ψ, is proportional to the amount of crystalline material present

$$\psi = \frac{\left(\frac{I_{\text{diff}}}{I_{\text{trans}}}\right) \text{ at } t = t_{\text{irr}}}{\left(\frac{I_{\text{diff}}}{I_{\text{trans}}}\right) \text{ at } t = 0} \tag{3}$$

ψ ranges from one to zero as the material changes from crystalline to amorphous. As shown in Fig. 4, ψ remains close to one throughout the irradiation, decreasing sharply at the end. This behavior suggests that the C-A transformation occurs relatively quickly throughout the entire precipitate near the end of irradiation time. This occurrence implies that the kinetics of amorphization are fast compared to the irradiation time and that the thermodynamic driving force controls the observed behavior.

What causes the small variation in ψ before amorphization is unclear, but could be due to the nucleation and growth of small regions of amorphous material. Alternatively, the cause could be an artifact of the experiment caused by the Gaussian shape of the beam that deposits a higher dose at the center than at the outer edges. There is some evidence for the latter mechanism since in some cases an amorphous region was first observed at the center of the beam, then slowly spread outward.

The model presented below emphasizes the development of the thermodynamic driving force for amorphization.

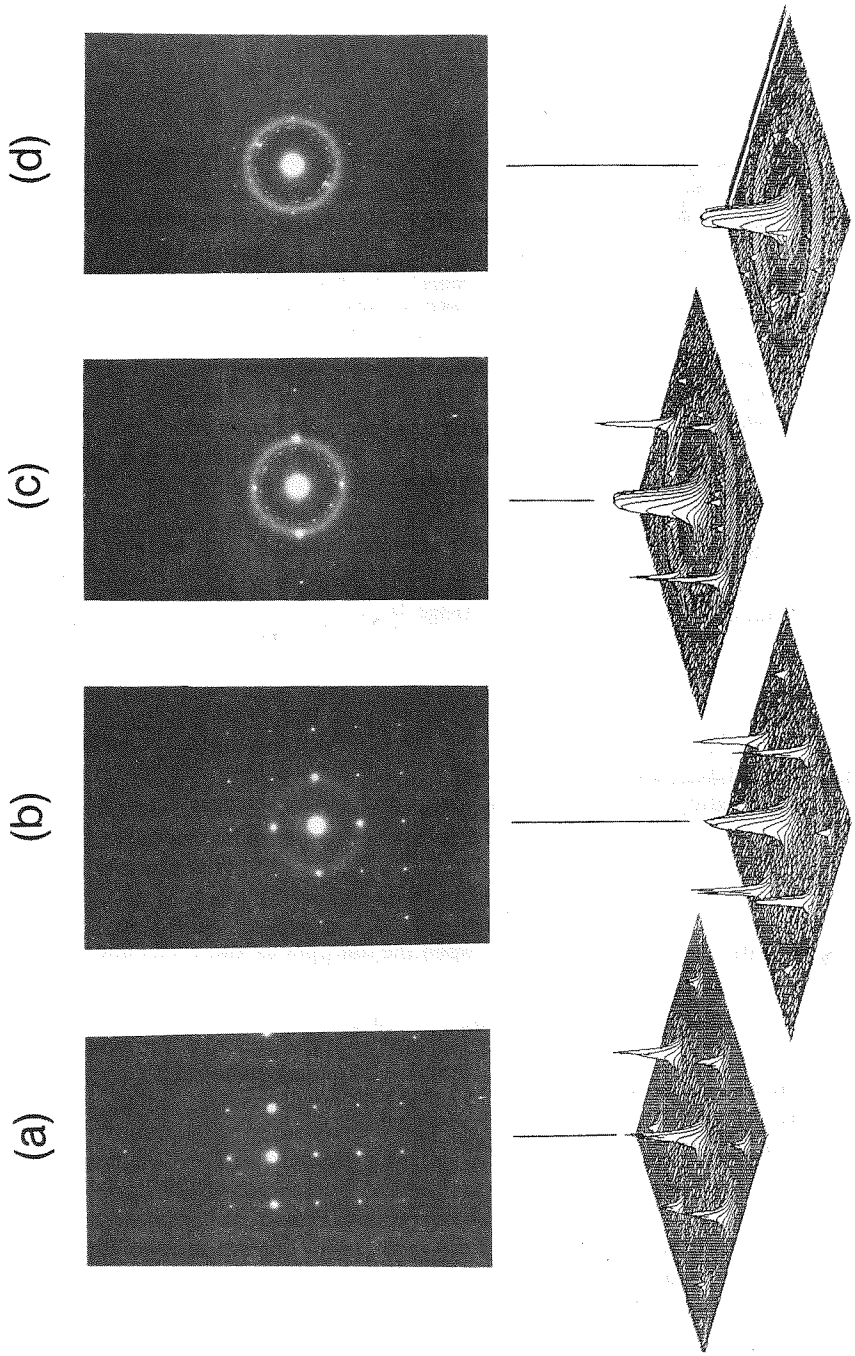

FIG. 3—*Diffraction pattern series of an amorphization experiment, with the corresponding intensity maps. Note the gradual emergence of a ring pattern accompanied by a decrease in the diffracted spot intensities. For this case* $T = 283$ *K, and* $k = 3.74 \times 10^{-2}$. *The fluences are 0 dpa in* (a) *9.1 in* (b), *15.7 in* (c) *and 19.1 in* (d).

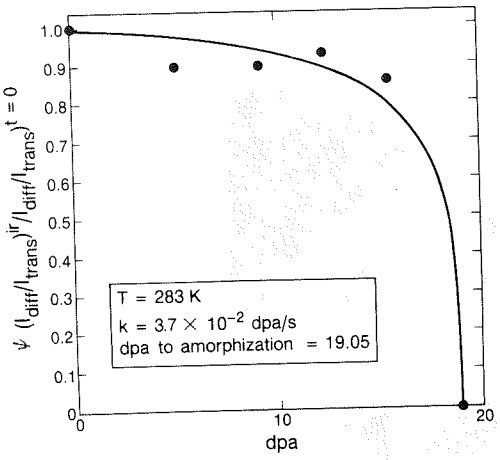

FIG. 4—*Crystalline volume fraction ψ versus dpa.*

Theory

The C-A transformation is assumed to occur because an increase in the free energy of the crystalline phase due to irradiation renders it unstable with respect to the amorphous phase. The irradiation-induced free energy change is

$$\Delta G_{irr} = G_c^{irr} - G_c = \Delta G_{def} + \Delta G_{dis} \tag{4}$$

where the subscript c stands for crystalline, G_c^{irr} is the free energy of the irradiated crystalline phase, and ΔG_{def} and ΔG_{dis} are the increases in free energy due to the accumulation of point defects and to irradiation-induced disorder, respectively. The amorphization condition is then

$$\Delta G_{irr} \geq \Delta G_{ac} \tag{5}$$

where G_a is the difference in free energy between the amorphous and crystalline states

$$\Delta G_{ac} = \Delta H_{ac} - T_{irr}\Delta S_{ac} \tag{6}$$

where ΔH_{ac} is the heat of crystallization for Zr_2Ni [7]. ΔS_{ac} is estimated by the entropy change at melting. This approximation is based on the close similarity of the structure, or lack thereof, of an amorphous solid and a liquid

$$\Delta S_{ac} \approx \Delta S_{melt} = \frac{\Delta H_{melt}}{T_{melt}} \tag{7}$$

Eq 6 is then

$$\Delta G_{ac} = \Delta H_{ac} - \Delta H_{melt}\left(\frac{T_{irr}}{T_{melt}}\right) \tag{8}$$

Calculation of Free Energy Change due to Point Defect Accumulation

The change in free energy due to point defect accumulation can be written as

$$\Delta G_{\text{def}} = \Delta H_{\text{def}} - T_{\text{irr}}\Delta S_{\text{def}} = \sum_{j=i,v} C_{jj}\Omega_j + RT_{\text{irr}}(C_j \ln C_j + (1 - C_j)\ln(1 - C_j)) \quad (9)$$

where C_j is the concentration of defect species j and Ω_j is the energy associated with its formation.

To find the concentration of point defects as a function of time the transient point defect balances must be solved. Other studies have solved the point defect balances for thin foils but they either considered a steady state case [*8*] or did not allow for diffusion to surface sinks [*9*]. Another paper in this conference [*10*] uses rate theory to calculate the point defect balances and arrives at conclusions similar to the ones presented below.

The thickness L is assumed to be much smaller than the beam diameter so that the defect concentrations are dependent only on x, the distance from the foil midplane. As mentioned above, the dpa to produce amorphization is comparable for both bulk and precipitate $Zr_2(Ni,Fe)$. This lends credence to this approximation, which ignores the zirconium matrix surrounding the precipitate. The problem can then be modeled by the slab geometry as shown in Fig. 5.

The interstitial and vacancy concentrations in the foil are governed by

$$\frac{\partial C_v}{\partial t} = D_v \frac{\partial^2 C_v}{\partial x^2} + k - K_{\text{iv}} C_i C_v \quad (10)$$

$$\frac{\partial C_i}{\partial t} = D_i \frac{\partial^2 C_i}{\partial x^2} + k - K_{\text{iv}} C_i C_v \quad (11)$$

where D_i and D_v are the respective point defect diffusion coefficients, k is the defect production rate, and K_{iv} is the recombination coefficient. Eqs 10 and 11 are solved with the following initial and boundary conditions

$$C_i = C_v = 0 \text{ at } t = 0 \text{ for all } x \quad (12)$$

$$C_i = C_v = 0 \text{ at } x = L \text{ for all } t \quad (13)$$

$$\frac{\partial C_v}{\partial x} = \frac{\partial C_i}{\partial x} = 0 \text{ at } x = 0 \text{ for all } t \quad (14)$$

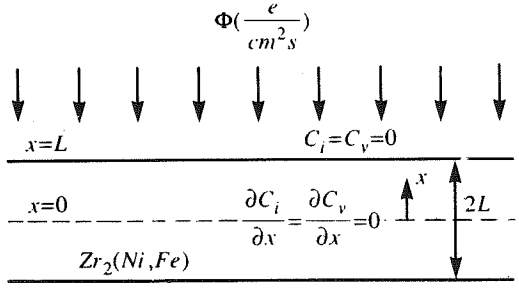

FIG. 5—*Geometry for solving point defect balances.*

where L is the foil half-thickness. This system of equations can be non-dimensionalized as

$$\Gamma \frac{\partial y_v}{\partial \tau} = \epsilon \frac{\partial^2 y_v}{\partial \chi^2} + 1 - y_i y_v \tag{15}$$

$$\frac{1}{\Gamma} \frac{\partial y_i}{\partial \tau} = \epsilon \frac{\partial^2 y_i}{\partial \chi^2} + 1 - y_i y_v \tag{16}$$

with the initial and boundary conditions

$$y_i = y_v = 0 \text{ at } t = 0 \tag{17}$$

$$y_i = y_v = 0 \text{ at } \chi = 1 \tag{18}$$

$$\frac{\partial y_v}{\partial \chi} = \frac{\partial y_i}{\partial \chi} = 0 \text{ at } \chi = 0 \tag{19}$$

The dimensionless variables are defined as follows

$$y_i = \sqrt{\frac{B_i}{B_v}}\,\Theta_i \qquad \Theta_i = \sqrt{\frac{K_{iv}}{k}}\,C_i \tag{20}$$

$$y_v = \sqrt{\frac{B_v}{B_i}}\,\Theta_v \qquad \Theta_v = \sqrt{\frac{K_{iv}}{k}}\,C_v \tag{21}$$

$$B_i = \frac{D_i}{L^2\sqrt{K_{iv}}} \qquad B_v = \frac{D_v}{L^2\sqrt{K_{iv}}} \qquad \Gamma = \sqrt{\frac{B_i}{B_v}} \tag{22}$$

$$\tau = \sqrt{K_{iv}}kt \qquad \epsilon = \sqrt{B_i B_v} \qquad \chi = \frac{x}{L} \tag{23}$$

The system of Eqs 15 through 19 was solved numerically. The vacancy concentrations were found to be several orders of magnitude bigger than the interstitial concentrations. The explanation is that the larger mobility of the interstitials allows them to escape to the surface while the vacancies are eliminated only through recombination. In Fig. 6 the concentration of vacancies is plotted as a function of distance from the foil midplane for several times τ and a fixed Γ. One can see that the spatial gradients are not very large; the concentrations never vary by more than a factor of 2 across the foil thickness except for the expected drop at the surface. These results mean that the whole foil reaches comparable concentrations of defects simultaneously, which agrees with the shape of Fig. 4.

In Fig. 7 Θ_v at $\chi = 0$ is plotted against time for several values of Γ. The curves for different Γ differ only in their final steady state. For the experimental cases of interest, a steady state is not reached before amorphization. For $\tau > 10$, all curves follow a common straight line on a log-log plot

$$\Theta_v = 3.9\tau^{1/2} \tag{24}$$

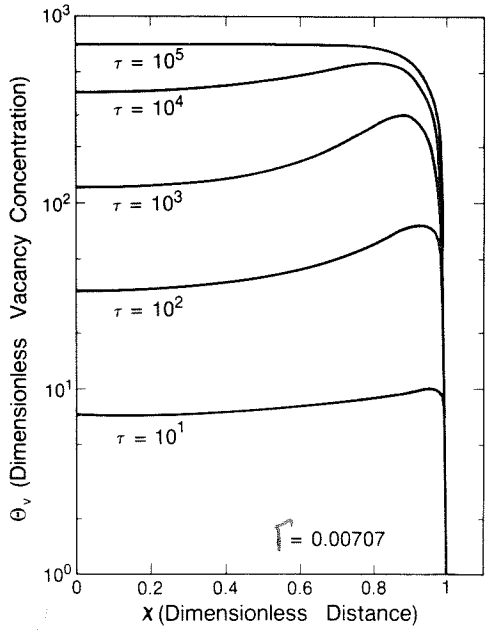

FIG. 6—*Dimensionless vacancy concentration as a function of distance from midplane of foil, for several times* τ.

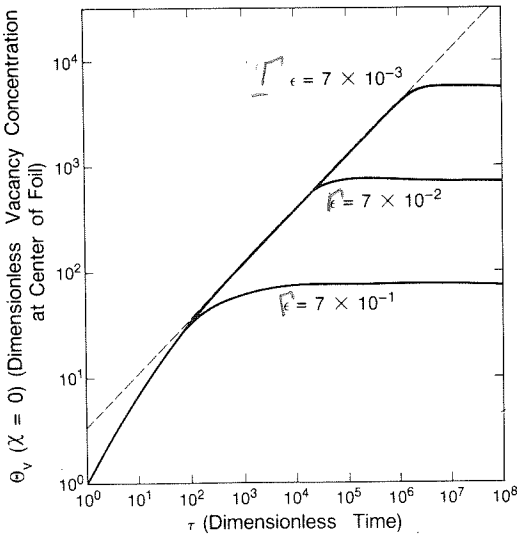

FIG. 7—*Dimensionless vacancy concentration as a function of dimensionless time for several values of* ϵ. *The dashed line is the linear approximation of Eq 24.*

or, using dimensional variables

$$C_v = 3.9 \left(\frac{k}{K_{iv}}\right)^{1/4} \sqrt{kt} \tag{25}$$

Eq 25 shows that C_v has, in addition to a square root dependence on the fluence, a one-fourth power dependence on k and K_{iv}. For high dose rates, the precipitates are therefore predicted to amorphize more quickly, since C_v will be higher for a given fluence, compared to a low dose rate case. Since K_{iv} is dependent on the temperature through the diffusion coefficient, C_v drops exponentially with temperature, and therefore causes the dose to amorphization to rise exponentially, as observed experimentally.

This calculation predicts $C_v \approx 10^{-2}$ at the end of the irradiation time. That the lattice can hold as many vacancies is due to the fact that the vacancies are immobile while the mobile interstitials are annihilated at the surface sink. The vacancy concentration should therefore rise until there are so many vacancies that every newly created interstitial falls within the recombination volume of a vacancy. Recombinatory numbers are usually taken to be ≈50 [*11*] which would give a maximum C_v of 0.02.

Calculation of the Free Energy Change due to Disordering

In order to calculate the disordering contribution on Eq 4, ΔG_{dis} must be specified in terms of the degree of order in the system as a function of dose. The long-range order parameter S will be assumed to be the sole determinant of the state of order. S is defined by

$$S = \frac{F_{aa} - x_a}{1 - x_a} \tag{26}$$

where F_{aa} is the probability of finding a Type A atom on a Type A lattice site and x_a is the atom fraction of A. For a binary alloy, we can analogously write the following quantities in terms of S

$$F_{bb} = x_b + S(1 - x_b) \tag{27}$$

$$F_{ab} = x_a(1 - S) \tag{28}$$

$$F_{ba} = x_b(1 - S) \tag{29}$$

where F_{bb}, F_{ab} and F_{ba} are the probabilities of finding a B atom on a B site, an A atom on a B site, and a B atom on an A site, respectively. If there is no short-range ordering, the number of AB bonds is

$$C_{pab} = F_{aa}(Z_{ba}F_{bb} + Z_{aa}F_{ba}) + F_{ab}(Z_{bb}F_{bb} + Z_{ab}F_{ba}) \tag{30}$$

where the Z_{nm} are the number of n type nearest neighbor sites around m type sites. C_{pab} can be written in terms of S by substituting Eqs 26 to 29 into Eq 30. For an ordering material C_{pab} will decrease as S decreases. Assuming $S = 1$ (perfect order) at the beginning of

irradiation, the variation in the number of AB bonds is given by

$$\Delta C_{\text{pab}} = C_{\text{pab}}(S) - C_{\text{pab}}(1) = A_2(1 - S^2) + A_1(1 - S) \tag{31}$$

where A_1 and A_2 are constants that depend on the crystal structure and stoichiometry of the alloy. The mixing enthalpy is then

$$\Delta H_{\text{dis}} = NV\Delta C_{\text{pab}} \tag{32}$$

where N is the total number of lattice sites per mol and V is the ordering energy.

The Frenkel pairs formed by irradiation recombine almost randomly, since the defect formation energies are much bigger than the ordering energy. The random recombination mechanism above can be shown [*12,13*] to cause S to decrease according to

$$\left(\frac{dS}{dt}\right)_{\text{irr}} = -kS \tag{33}$$

The opposing thermal reordering term was evaluated by making a balance of the ordering and disordering thermal jump rates for a vacancy mechanism. For the temperatures of interest, vacancy thermal reordering was found to be negligible if the vacancy migration energy is of the order of 1 eV. S can then be calculated by integrating Eq 33

$$S(t) = S_0 e^{-kt} \tag{34}$$

ΔS_{dis} is a configurational entropy given by [*14*]

$$\Delta S_{\text{dis}} = R(C_{aa}\ln C_{aa} + C_{ab}\ln C_{ab} + C_{ba}\ln C_{ba} + C_{bb}\ln C_{bb}) \tag{35}$$

where C_{ab}, C_{ba}, C_{bb}, and C_{aa} are the concentrations of A atoms on B sites, B atoms on A sites, B atoms on B sites, and A atoms on A sites, respectively. The disordering free energy

$$\Delta G_{\text{dis}} = \Delta H_{\text{dis}} - T_{\text{irr}}\Delta S_{\text{dis}} \tag{36}$$

is a function of the ordering parameter S by Eqs 32 and 35.

Calculation of the Total Free Energy Change and Prediction of Amorphization

The total free energy change is

$$\begin{aligned}\Delta G_{\text{irr}} = &\sum_{k=i,v}(C_k\Omega_k + RT_{\text{irr}}(C_k\ln C_k + (1 - C_k)\ln(1 - C_k)) \\ &+ NV(A_2(1 - S^2) + A_1(1 - S)) - RT_{\text{irr}}\sum_{i=a,b}\sum_{j=a,b} C_{ij}\ln C_{ij}\end{aligned} \tag{37}$$

To calculate ΔG_{irr} from Eq 37, the migration energies of the point defects as well as the ordering energy need to be specified. The parameters used in the calculation are summarized in Table 1. E_v, E_i, and V were used as fitting parameters. None of these values is readily available for $Zr_2(Ni,Fe)$, so a direct comparison is difficult. The values arrived at (Table 1) are reasonable for intermetallic compounds [*9,15*]. The value arrived at for V compares very well with the estimate of the ordering energy for Zr_2Ni of 0.0265 eV given in Ref *16*.

TABLE 1—*Values for intermetallic compounds.*

Ω_i	interstitial formation energy = 4 eV
Ω_v	vacancy formation energy = 1 eV
E_i	interstitial migration energy = 0.4 eV
E_v	vacancy migration energy = 1.4 eV
V	ordering energy = 0.025 eV
K_{iv}	recombination coefficient = 3×10^{16} $(D_i + D_v)$
D_{io}	pre-exponential factor = 10, cm^2/s
D_{vo}	pre-exponential factor = 146, cm^2/s

The increase in free energy with irradiation dose for a typical case is shown in Fig. 8. The contributions due to the buildup of point defects and radiation-induced disordering are equally important. Interestingly, note that ΔG_{dis} rises sharply and subsequently levels off. At that point S is close to zero, which means that the precipitate disorders completely before amorphizing, as observed by Luzzi et al. [5].

The value of ΔG_{irr} given by Eq 37 is compared with ΔG_{ac} from Eq 8; when the condition expressed in Eq 5 is satisfied, the transformation occurs. This procedure yields a set of curves of dose to amorphization versus temperature, for each k, that can be fitted to the data. This theoretical model is shown in Fig. 2. The fit obtained, as is apparent, is quite good for reasonable values of the fitting parameters E_i, E_v and V.

Conclusions

A model has been proposed to predict the occurrence of the C-A transformation. The model is based on the kinetic evolution of the thermodynamic conditions for the transformation. A quantitative fit to the amorphization data has been achieved that includes the effect of dose rate. The amorphization models proposed in the literature [*17–19*] are basically thermodynamic in nature. They differ in the mechanism responsible for energy storage in

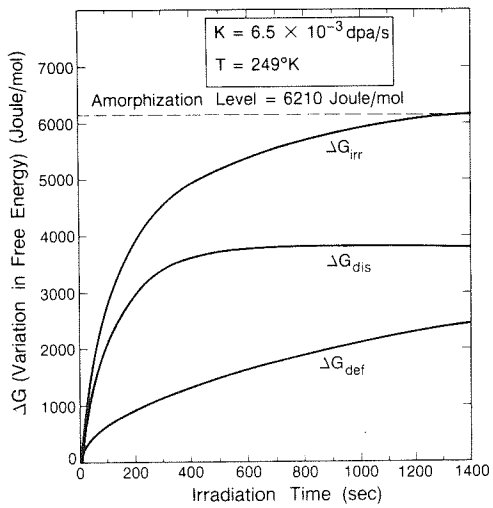

FIG. 8—*Precipitate total free energy as a function of irradiation time. The two free energy components, due to disordering and to defects, are also indicated, as well as the amorphization level.*

the lattice (that is, point defect buildup or radiation-induced disordering). This work indicates that, at least for the case of electron-irradiated thin foils, both mechanisms are equally important.

The significant role played by the surface sink in the point defect balances indicates that utmost care is necessary in simulating neutron and high energy proton irradiation with electron irradiation. Surface effects are an inherent part of electron irradiation of thin foils but are not present in bulk irradiation.

Acknowledgments

This work was partially sponsored by the Electric Power Research Institute (EPRI) under contract number RP-1250-14, and supported in part by the Director, Office of Energy Research, Office of Basic Energy Science, Materials Science Division of the U.S. Department of Energy under Contract Number DE-AC03-76SF00098. The financial support received from the Brazilian National Research Council (CNPq) by one of us (A. T. Motta) is gratefully acknowledged.

References

[1] Griffiths, M., Gilbert, R. W., and Carpenter, G. J. C., *Journal of Nuclear Materials,* Vol. 150, 1987, p. 53.
[2] Yang, W. J. S., Tucker, R. P., Cheng, B., and Adamson, R. B., *Journal of Nuclear Materials,* Vol. 138, 1986, p. 185.
[3] Oen, O. S., "Cross Sections for Atomic Displacements in Solids by Fast Electrons," Report 4897, Oak Ridge National Laboratory, Oak Ridge, TN, 1973.
[4] Mori, H., Fujita, H., Tendo, M., and Fujita, M., *Scripta Metallurgica,* Vol. 18, 1984, p. 783.
[5] Luzzi, D. E., Mori, H., Fujita, H., and Meshii, M., *Acta Metallurgica,* Vol. 34, 1986, p. 629.
[6] Luzzi, D. E., Mori, H., Fujita, H., and Meshii, M., *Scripta Metallurgica,* Vol. 18, 1984, p. 957.
[7] Henaff, M. P., Colinet, C., Pasturel, A., Buschow, K. H. J., *Journal of Applied Physics,* Vol. 56, 1984, p. 307.
[8] White, R. J., Fisher, S. B., Miller, K. M., *Radiation Effects,* Vol. 41, 1979, p. 17.
[9] Simonen, E., *Nuclear Instruments and Methods,* Vol. B16, 1986, p. 198.
[10] Hashimoto, T., this volume, pp. 523–538.
[11] Fuse, M., *Journal of Nuclear Materials,* Vol. 136, 1985, p. 250.
[12] Aronin, L. R., *Journal of Applied Physics,* Vol. 25, 1954, p. 344.
[13] Kirk, M. A. and Blewitt, T. H., *Metallurgical Transactions, A,* Vol. 9, 1978, p. 1729.
[14] Gordon, P., *Principles of Phase Diagrams,* McGraw-Hill, New York, 1968.
[15] Banerjee, S. and Urban, K., *Physica Status Solidii,* Vol. 81, 1984, p. 145.
[16] Luzzi, D. and Meshii, M., *Research Mechanica,* Vol. 21, 1987, p. 207.
[17] Cahn, R. W. and Johnson, W. L., *Journal of Materials Research,* Vol. 1, 1986, p. 724.
[18] Luzzi, D. E. and Meshii, M., *Journal of Materials Research,* Vol. 1, 1986, p. 617.
[19] Limoge, Y. and Barbu, A., *Physical Review B,* Vol. 30, 1984, p. 2212.